

**NUMERICAL CALCULATION OF
UNSTABLE IMMISCIBLE FLUID DISPLACEMENT
IN A TWO-DIMENSIONAL POROUS MEDIUM
OR HELE-SHAW CELL**

M. R. DAVIDSON¹

(Received 30 May 1983; revised 6 March 1984)

Abstract

A numerical procedure for calculating the evolution of a periodic interface between two immiscible fluids flowing in a two-dimensional porous medium or Hele-Shaw cell is described. The motion of the interface is determined in a stepwise manner with its new velocity at each time step being derived as a numerical solution of a boundary integral equation. Attention is focused on the case of unstable displacement characterised physically by the “fingering” of the interface and computationally by the growth of numerical errors regardless of the numerical method employed. Here the growth of such errors is reduced and the usable part of the calculation extended to finite amplitudes. Numerical results are compared with an exact “finger” solution and the calculated behaviour of an initial sinusoidal displacement, as a function of interfacial tension, initial amplitude and wavelength, is discussed.

1. Introduction

In a recent paper, the author [3] derived an integral equation for the normal velocity of the interface between two immiscible, viscous fluids in a two-dimensional porous layer or Hele-Shaw cell when one of the fluids is displaced vertically by the other. This equation was expressed in terms of the physical parameters, a Green’s function and the interface itself.

¹ CSIRO Division of Mineral Physics, Lucas Heights Research Laboratories. Private Mail Bag 7, Sutherland, N.S.W. 2232.

© Copyright Australian Mathematical Society 1985, Serial-fee code 0334-2700/85

If there were no numerical errors then, in principle, a stepwise numerical procedure could be used to determine completely the evolution of the interface, from some initial configuration, by progressively solving the integral equation for the normal velocity at each point on the interface at each time step. For stable flows in which small perturbations of the interface decay with time, this process should present no problems beyond those of ensuring accuracy and computational stability. More challenging is the case of unstable flows for which numerical perturbations of the interface must grow, along with the desired solution, regardless of the computational method. The objective in such cases is to delay, for as long as possible, the inevitable onset of numerical instability. Physically, these unstable flows are characterised by the development of fingers of displacing fluid which penetrate the displaced fluid region, and are of interest in a number of contexts (*e.g.* oil recovery, groundwater movement).

Conditions governing the onset of instability of an initially plane interface have been derived by Saffman and Taylor [9] and Chuoke *et al.* [2] using a first order perturbation analysis which is valid for small amplitudes. These authors showed that, for a small perturbation,

$$y = \varepsilon \exp(inx + \sigma t),$$

of the undisturbed interface $y = 0$,

$$(\mu_1 + \mu_2)\sigma/n = (\mu_1 - \mu_2)V + \kappa g(\rho_1 - \rho_2) - n^2\gamma\kappa, \quad (1)$$

and hence this disturbance is unstable ($\sigma > 0$) when its wavelength $\lambda = 2\pi/n$ is greater than the critical value λ_c where

$$\lambda_c^2 = 4\pi^2\gamma/(V(\mu_1 - \mu_2)/\kappa + g(\rho_1 - \rho_2)) \quad (2)$$

whenever the denominator is positive. Motion is upward with uniform velocity V and (x, y) are rectangular coordinates with y being the upward vertical. Suffix 1 refers to the upper fluid and suffix 2 to the lower, and μ, ρ, γ denote fluid viscosity density and interfacial tension, respectively. The permeability of the medium is taken to be the same (κ) for both fluids and g is the acceleration due to gravity.

In this paper, the medium is considered to be infinitely long with width L where L represents the half period of a periodic interface of infinite extent. A numerical technique is described which successfully traces the unstable growth of the interface up to amplitudes which can be much greater than those for which a perturbation analysis is valid. The objective is first to extend the means available for investigating theoretically the growth of an unstable interface, and second to examine in detail the growth behaviour of an initial sinusoidal disturbance using this technique.

2. The integral equation

The macroscopic interface (C) separating the two fluids is assumed to be sharp. Across this interface the normal velocity is continuous and a pressure jump is chosen with the form

$$p_2 - p_1 = \gamma H(x, y) + P_c$$

where H is the macroscopic curvature of the interface and P_c is a constant “capillary” pressure associated with the microscopic interfaces underlying C . Neumann conditions apply at the side walls $x = 0$ and $x = L$, and the motion at large distances upstream and downstream is taken to be uniform with velocity V . The governing equation, $\nabla^2 p_i = 0$, is determined by Darcy’s Law in each fluid ($i = 1, 2$) together with continuity when the densities ρ_i are constant. In the case of a Hele-Shaw cell, the thickness averaged flow equations are mathematically analogous to Darcy’s Law.

Davidson [3] uses the Green’s function

$$G(x, y; \zeta, \eta) = \frac{1}{4\pi} \log \left(\cosh \frac{\pi}{L} (y - \eta) - \cos \frac{\pi}{L} (x + \xi) \right) \left(\cosh \frac{\pi}{L} (y - \eta) - \cos \frac{\pi}{L} (x - \zeta) \right) \quad (3)$$

which satisfies the side wall boundary conditions, to derive the following integral equation for the normal velocity (U_n) of the interface in the above problem:

$$U_n(X) = V \cos \theta(X) + 2 \int_C F(\xi) \frac{\partial G(X; \xi)}{\partial n(X)} ds(\xi) - \frac{2\gamma\kappa}{\mu_1 + \mu_2} \left(\int_C M(X; \xi) ds(\xi) - \frac{dH(X)}{ds} (G(X; \xi))_{\xi=0}^L \right),$$

with

$$F(\xi) = \left(\frac{\mu_1 - \mu_2}{\mu_1 + \mu_2} \right) U_n(\xi) + \kappa g \left(\frac{\rho_1 - \rho_2}{\mu_1 + \mu_2} \right) \cos \theta(\xi) \quad (4)$$

and

$$M(X; \xi) = (H(\xi) - H(X)) \frac{\partial^2 G}{\partial n(X) \partial n(\xi)} + \frac{dH(X)}{ds} \frac{\partial G}{\partial s(\xi)}$$

where the normal n is directed from the lower to the upper fluid, θ is the angle between the normal and the positive y axis, s denotes arc length and X and ξ denote, respectively, (x, y) and (ζ, η) . By symmetry about the side walls, $\theta = dH/ds = 0$ at the end points of C . The reader is referred to [3] for details of the model assumptions and analysis leading to equation (4).

We use equations (A1) to (A2) (see Appendix), to derive the following alternative form of equation (4):

$$U_n(X) = V \cos \theta(X) + 2 \int_C \left(F(\xi) \frac{\partial G}{\partial n(X)} - F(X) \frac{\partial G}{\partial n(\xi)} \right) ds(\xi) + \frac{2\gamma\kappa}{\mu_1 + \mu_2} \int_C Q(X; \xi) ds(\xi) \quad (5)$$

where

$$Q(X; \xi) = \frac{dH(X)/ds}{\cos \theta(X)} \left(\cos \theta(\xi) \frac{\partial G}{\partial s(X)} - (\eta - y) \frac{\partial^2 G}{\partial s(X) \partial n(\xi)} \right) - (H(\xi) - H(X)) \frac{\partial^2 G}{\partial n(X) \partial n(\xi)}.$$

When $\xi = X$,

$$\frac{\partial G}{\partial n(X)} = \frac{\partial G}{\partial n(\xi)} = \frac{H}{4\pi} - \frac{\sin \theta}{4L} \cot \frac{\pi x}{L}$$

and

$$Q(X; X) = \frac{1}{4\pi} (H_{xx} \cos^2 \theta - HH_x \sin \theta) + \frac{1}{4L} H_x \cot \frac{\pi x}{L} \cos^2 \theta.$$

If the interface is described by a single valued function $y(x, t)$ then, along lines of constant x , its motion may be expressed as

$$\partial y / \partial t = U_n / \cos \theta. \quad (6a)$$

The numerical procedure described in section (3) is presented in terms of this case, but it applies analogously in the more general case when C is expressed parametrically and the motion may be determined by following points $(x(s, t), y(s, t))$ on C which satisfy

$$\frac{dx}{dt} = -U_n \sin \theta, \quad \frac{dy}{dt} = U_n \cos \theta. \quad (6b)$$

Given an initial displacement of the interface, the objective is to use equations (5) and (6a) to follow numerically the position of the interface with time for as long as the growth of numerical errors permits. For reasons to be discussed in the next section, it is important to use equation (5) rather than equation (4) during time stepping.

3. The numerical method

We solve equations (5) and (6a) along equally spaced lines $x = x_j = j\Delta x$ ($j = 0, 1, \dots, N$). On each line $x = x_j$, we use the Adams-Bashforth-Moulton scheme (see Hamming [6]), applied to equation (6a), to advance through time with

local errors of order $(\Delta t)^5$ where Δt is the time step. Then

$$y_{1p} = y_0 + \frac{\Delta t}{24}(55y'_0 - 59y'_{-1} + 37y'_{-2} - 9y'_{-3})$$

and

$$y_{1c} = y_0 + \frac{\Delta t}{24}(9y'_{1p} + 19y'_0 - 5y'_{-1} + y'_{-2})$$

where ' denotes $\partial/\partial t$, y_k denotes $y(x_j, t + k\Delta t)$ and y_{1p}, y_{1c} denote predicted and corrected values of y_1 . A fourth order Runge-Kutta formula is used to start the process.

At each time step, quadrature of the integral in equation (5) (in terms of variable x) using Simpson's rule followed by collocation at $x = x_j$ gives a set of simultaneous linear algebraic equations, having errors of order $(\Delta x)^4$, for the values of U_n . When $\gamma = 0$, the form of the first integral in equation (5) avoids the need to determine H and also numerically conserves mass following quadrature of the integral. When $\gamma \neq 0$, both the slope and the curvature together with its first two derivatives are required to be determined.

Davidson [3] solved equation (4) for U_n corresponding to example interfaces which were known analytically. However during time stepping, the interface is only known approximately and the term $\cot \pi x/L$ in $M(X; X)$ and $\partial G/\partial n(X)$ and the logarithmic singularity in $(G(X; \xi))_{\xi=0}^L$ can lead to the catastrophic growth of errors near the side walls if equation (4) is used. Equation (5) eliminates this difficulty in the first and last terms of equation (4); however the term $\cot \pi x/L$ in $Q(X; X)$ remains. This suggests a truncated Fourier series approximation for H_x so that, if

$$H_x = \frac{-\pi}{L} \sum_{k=1}^K ka_k \sin \frac{k\pi x}{L} \tag{7}$$

where

$$a_k = \frac{2}{L} \int_0^L H(x) \cos \frac{k\pi x}{L} dx, \tag{8}$$

then the product $H_x \cot \pi x/L$ in $Q(X; X)$ becomes

$$-\frac{\pi}{L} \cos \frac{\pi x}{L} \sum_{k=1}^K ka_k f_k(x), \tag{9}$$

where the functions

$$f_k(x) = \sin(k\pi x/L)/\sin(\pi x/L)$$

can be evaluated in several forms which avoid any computational difficulty near $x = 0$ or L (see *e.g.* Gradshteyn and Ryzhik [4], page 27). One such form is

$$f_k(x) = \sum_{i=1}^I (-1)^{i-1} \binom{k-i}{i-1} \left(2 \cos \frac{\pi x}{L}\right)^{k-2i+1} \tag{10}$$

where

$$I = \begin{cases} \frac{1}{2}(k + 1), & k \text{ odd,} \\ \frac{1}{2}k, & k \text{ even.} \end{cases}$$

We choose here to calculate the slope and the curvature of the interface at each time step by the use of cubic splines. The recommended procedure (Ahlberg *et al.* [1]) is to first derive the slope by spline fitting $y(x_j)$ and then to spline fit the slopes themselves and use the resulting derivatives as the required $y_{xx}(x_j)$ for determining the curvature $H(x_j)$.

Having obtained the curvature we integrate equation (8) numerically (Simpson's rule) to give the Fourier coefficients a_k . Derivatives of curvature H_x and H_{xx} are now estimated from equation (7), and it is also important to re-evaluate $H(x_j)$ according to

$$H(x) = a_0 + \sum_{k=1}^K a_k \cos \frac{k\pi x}{L} \quad (11)$$

so that the values for H and its derivatives used in the evaluation of $Q(X; \xi)$ are consistent. Failure to do this results in the rapid growth of errors arising from the cancellation of the singularities near $\xi = X$ in the terms involving $\partial G/\partial s(X)$ and $\partial^2 G/\partial n(X)\partial n(\xi)$.

During unstable flows, the rapid growth of numerical errors results in a calculated solution which develops a characteristic saw-toothed appearance. Here we draw on the numerical experiences of Longuet-Higgins and Cokelet [7] who calculated the motion of surface waves on water. These authors encountered a weak instability in their solution which they removed by smoothing; the exact curve was presumed to lie midway between two smooth curves passing through alternate points. In this paper we approximate the bounding upper and lower smooth curves separately by cubic splines, and carry out the smoothing at every time step.

An attempt to combine the elimination of high frequency error modes of y with a computationally suitable form for $H_x \cot \pi x/L$ by approximating y with a truncated Fourier series met with some success, but the method described here is more accurate and integrates the solution further.

4. Numerical accuracy

Saffman [10] considered the motion of a viscous fluid which is driven by a fluid of negligible viscosity ($\mu_2 = 0$) in the absence of gravity, and derived a family of exact solutions for the interface which are approximately sinusoidal at small times and are asymptotically equal to the Saffman-Taylor profile at large times. These

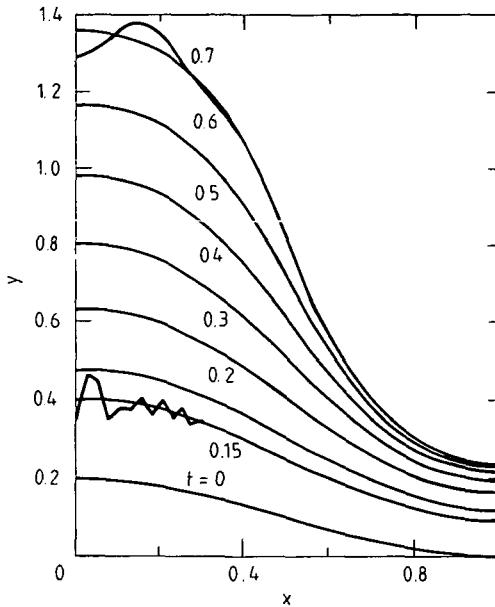


FIGURE 1. Comparison of exact and numerical solutions (with and without smoothing) for an initial Saffman interface with amplitude 0.1 where $V = L = 1$, $\mu_2 = 0$, gravity is ignored and $\gamma = 0$. The saw-toothed solution at $t = 0.15$ is an example of a numerically unsmoothed solution. For $t < 0.7$ the numerically smoothed and the exact solutions coincide and correspond to the curves shown. At $t = 0.7$, an oscillation appears near the nose of the numerically smoothed solution which now differs substantially from the exact curve.

solutions may be used to gauge directly the accuracy of our numerical procedure when $\gamma = 0$. Unfortunately, the author is unaware of any similar exact solution corresponding to $\gamma \neq 0$.

In Figure 1 numerical solutions for $\gamma = 0$ are compared with the corresponding exact Saffman profiles showing the development of the instability in the absence of smoothing and the subsequent improvement in the solution when smoothing is applied. In the latter case numerical errors still grow (as they must) but they do so much more slowly than before so that the solution may be integrated further. Similar behaviour occurs when $\gamma \neq 0$.

The difference $|y_{\text{smooth}} - y|_{\text{max}}$ is an index of the error growth in the numerical solution. It increases with time for unstable flows and is plotted in Figures 2 and 3 to illustrate the effect of changes in Δx and Δt . Alternatively, when $\gamma \neq 0$ we could monitor the error in the calculated mass balance which follows a similar pattern with time. However, when $\gamma = 0$, mass is conserved numerically. In the absence of smoothing, halving Δx from 0.05 to 0.025 accelerates the onset of the instability. However, when smoothing is applied, Figures 2 and 3 show that such a reduction in Δx reduces the error as does halving Δt from 0.003125 to 0.0015625.

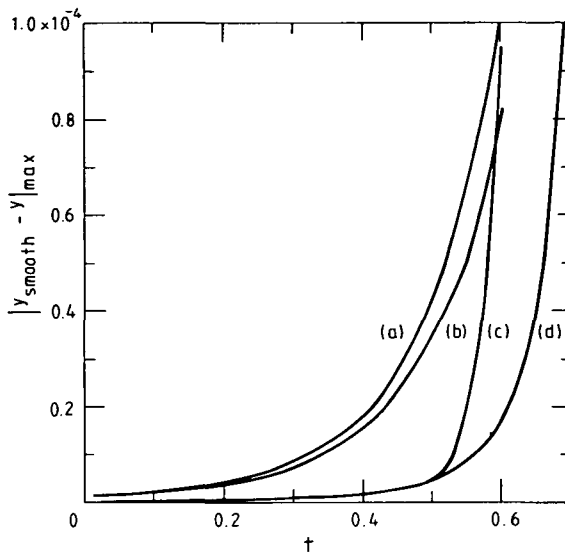


FIGURE 2. Error index versus time when $V = L = 1$, $\mu_2 = 0$, gravity is ignored and $\gamma = 0$ for an initial Saffman interface with amplitude 0.1. Curves (a)–(d) correspond to the following choices of Δx and Δt : (a) $\Delta x = 0.05$, $\Delta t = 0.003125$, (b) $\Delta x = 0.05$, $\Delta t = 0.0015625$, (c) $\Delta x = 0.025$, $\Delta t = 0.003125$, (d) $\Delta x = 0.025$, $\Delta t = 0.0015625$.

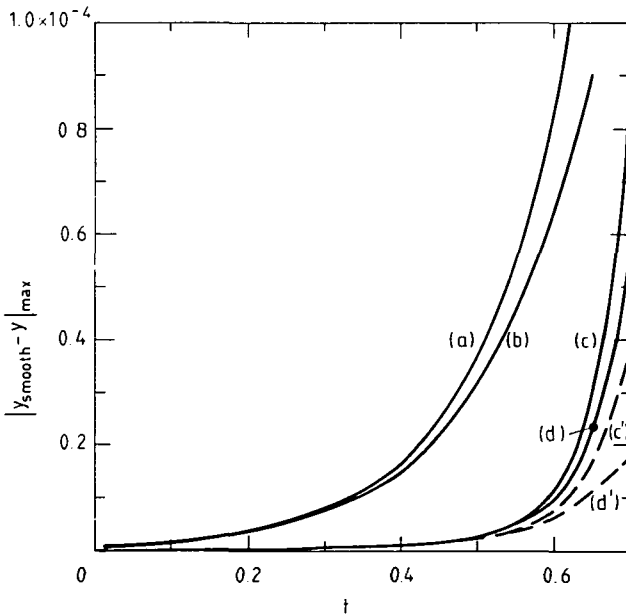


FIGURE 3. Error index versus time when $V = L = 1$, $\mu_2 = 0$, gravity is ignored and $\gamma\kappa/\mu_1 = 0.02$ for an initial interface $y = 0.1 \cos \pi x$. Solid curves (a)–(d) correspond to a choice of $K = 5$ Fourier components describing the curvature and to the following choices of Δx and Δt : (a) $\Delta x = 0.05$, $\Delta t = 0.003125$, (b) $\Delta x = 0.05$, $\Delta t = 0.0015625$, (c) $\Delta x = 0.025$, $\Delta t = 0.003125$, (d) $\Delta x = 0.025$, $\Delta t = 0.0015625$. The dashed curves (c') and (d') correspond to curves (c) and (d), respectively, with $K = 10$.

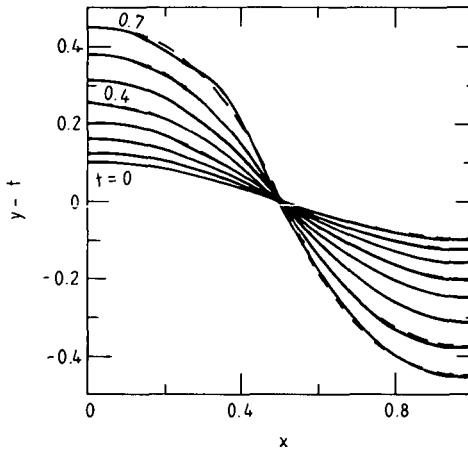


FIGURE 4. Displacement relative to the mean position versus x , plotted at time intervals of 0.1, when $V = L = 1$, $\mu_2 = 0$, gravity is ignored and $\gamma\kappa/\mu_1 = 0.02$ for an initial interface $y = 0.1 \cos \pi x$. The solid curves correspond to a choice of $K = 5$ Fourier components describing the curvature and the dashed curves correspond to $K = 10$.

Figure 3 also illustrates the error reduction which can be achieved by increasing the number of terms K (from 5 to 10) in the Fourier approximation of curvature and its derivatives (equations (7), (9), (11)) when $\gamma \neq 0$; the corresponding solution curves are compared in Figure 4. (Note that we must have $\Delta x < L/K$ for the computation to resolve the K th Fourier component.)

The calculation in Figures 3 and 4 corresponds to an initial cosine interface, with wavelength $\lambda = 2L$, and the physical parameters are in the unstable range (specifically, $\lambda_c/\lambda = \pi(0.02)^{1/2} < 1$). We found that when $K = 10$, smaller values of Δt with increasing λ_c/λ were required to achieve error growth rates similar to those in Figure 3. Furthermore, in the physically stable range $\lambda_c/\lambda > 1$ for small perturbations, there appears to be a restriction on Δt (perhaps analogous to a Courant condition) which ensures that the error decreases with time (note that, when $\lambda_c/\lambda > 1$, smoothing at each time step remains necessary, indicating that the basic formulation is still computationally unstable; however, in other stable regimes which occur when the denominator of equation (2) is negative, the calculation is also stable). The (unknown) bound on Δt presumably depends on Δx , K and the physical parameters. One can speculate that this same condition on Δt , together with a formulation (if such exists) which is computationally stable when $\lambda_c/\lambda > 1$, would also ensure “minimum” error growth rates in the physically unstable range.

Direct comparisons of numerical and exact Saffman solutions for $\gamma = 0$ indicate that they are almost indistinguishable when

$$|y_{\text{smooth}} - y|_{\text{max}} < 0.00004.$$

We now apply this criterion to define a valid calculation when $\gamma \neq 0$.

In Figures 5(a) and 5(b) the numerical solution for an initial displacement $y = \epsilon \cos \pi x/L$ is compared with the corresponding first order perturbation solution which has an error of only $O(\epsilon^3)$ rather than the expected $O(\epsilon^2)$ (Outmans [8]). The two solutions are almost identical when $t = 0.2$ but differences occur at larger times when a perturbation analysis becomes inapplicable.

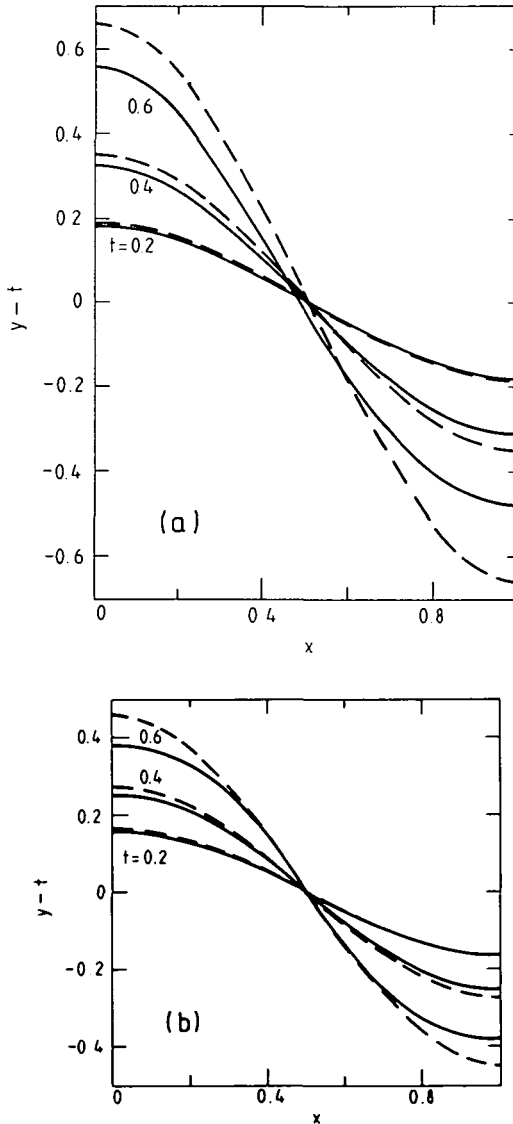


FIGURE 5. Comparison of numerical solutions (solid curves) and first order perturbation solutions (dashed curves) for an initial interface $y = 0.1 \cos \pi x$ when $V = L = 1$, $\mu_2 = 0$ and gravity is ignored. Results are plotted relative to the mean flow position. In (a) $\gamma = 0$ and in (b) $\gamma\kappa/\mu_1 = 0.02$.

In each case the amplitude growth rate is less than that predicted by the linear theory (a result also shown by Outmans [8] based on the inclusion of higher order terms) and the rate in Figure 5(b) ($\gamma \neq 0$) is less than that in Figure 5(a) ($\gamma = 0$) as is expected.

5. Dimensionless form

Rewritten in terms of dimensionless variables X/L and U_n/V , equation (5) contains three dimensionless parameters, *viz.*

$$\alpha_1 = \frac{\mu_1 - \mu_2}{\mu_1 + \mu_2}, \quad \alpha_2 = \frac{\kappa g}{V} \left(\frac{\rho_1 - \rho_2}{\mu_1 + \mu_2} \right), \quad \alpha_3 = \frac{\gamma \kappa}{L^2 V (\mu_1 + \mu_2)}.$$

If we also define dimensionless time by $\tau = (\alpha_1 + \alpha_2)Vt/L$ ($\alpha_1 + \alpha_2 > 0$ for unstable flows) and consider deviations of U_n and y about their mean values by setting $y^* = (y - Vt)/L$ and $W = (U_n/V - \cos \theta)/(\alpha_1 + \alpha_2)$ with $x^* = x/L$, then equations (5) and (6a) become

$$W = 2 \int_C \left(f(\xi) \frac{\partial G}{\partial n(X)} - f(X) \frac{\partial G}{\partial n(\xi)} \right) dx(\xi) + \frac{2\beta^2}{\pi^2} \int_C Q(X; \xi) ds(\xi) \tag{12}$$

and

$$\partial y^*/\partial \tau = W/\cos \theta \tag{13}$$

where $f = \alpha_1 W + \cos \theta$ and $\beta^2 = \pi^2 \alpha_3 / (\alpha_1 + \alpha_2)$, and the asterisks in equation (12) have been dropped for convenience. We see that these equations now involve explicitly only the two parameters α_1 and β . If the initial perturbation is sinusoidal with wavelength $\lambda = 2L$, then $\beta = \lambda_c/\lambda$.

6. Results

In this section we present and discuss results obtained by solving equations (12) and (13) with an initial cosine perturbation, having (dimensional) amplitude ϵL and wavelength $\lambda = 2L$ (*i.e.* $y^* = \epsilon \cos \pi x^*$ initially). Outmans [8] considered this case by performing a nonlinear perturbation analysis valid for small amplitudes.

Figure 6 shows results for $\alpha_1 = 1$, $\epsilon = 0.1$ and $\tau \leq 0.6$. We see that the nose velocity (V_N) increases with time and the tail velocity (V_T) decreases. When $\beta < 1$, $V_N > V_T$ and the profile amplitude increases; for $\beta > 1$, $V_N < V_T$ and the

amplitude decreases. These results agree with the stability criterion for small sinusoidal disturbances (equation 2). When $\beta = 1$ equation (2) predicts that the disturbance is neutrally stable (*i.e.* $\sigma = 0$); here $V_N < V_T$ initially and then changes to $V_N > V_T$ so that the amplitude increases slowly after an initial fall, an effect too small to be seen in Figure 6(b). We may check this behaviour for $\beta = 1$ against the corresponding perturbation solution which, in terms of our dimensionless variables, is

$$y^* = \varepsilon \cos \pi x^* + \frac{3}{8} \pi^2 \varepsilon^3 \left(\pi \tau \cos \pi x^* - \frac{1}{8} (1 - \exp(-24\pi\tau)) \cos 3\pi x^* \right) + O(\varepsilon^4). \tag{14}$$

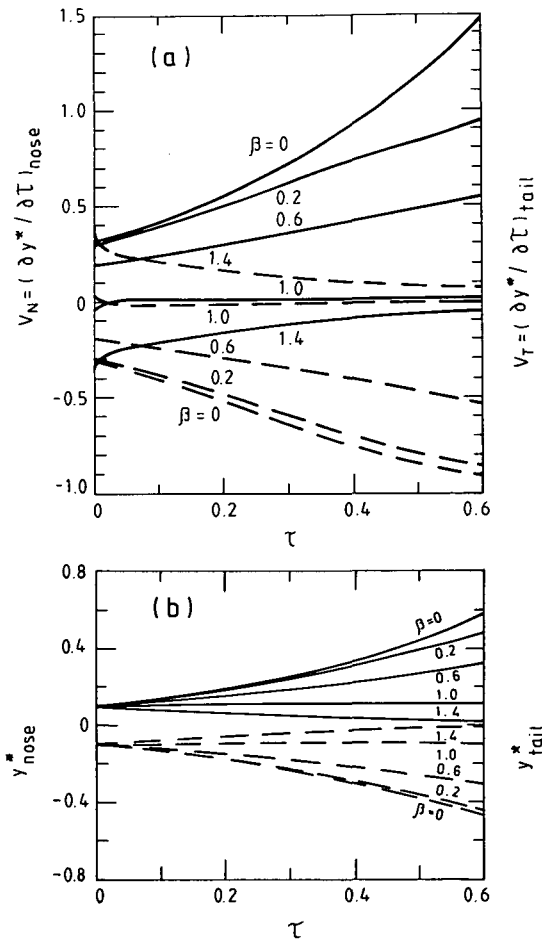


FIGURE 6. Development of an initial dimensionless displacement $y^* = 0.1 \cos \pi x^*$ when $\alpha_1 = 1$ for different values of $\beta = \lambda_c / \lambda$ where $y^* = (y - Vt) / L$, $x^* = x / L$ and $\lambda = 2L$. (a) Dimensionless nose velocity (solid lines) and tail velocity (dashed lines) $\partial y^* / \partial \tau$ relative to the mean flow versus dimensionless time $\tau = (\alpha_1 + \alpha_2) Vt / L$. (b) Dimensionless nose displacement (solid lines) and tail displacement (dashed lines) relative to the mean flow position versus τ . (c) Dimensionless displacement y^* versus x^* when $\tau = 0.6$.

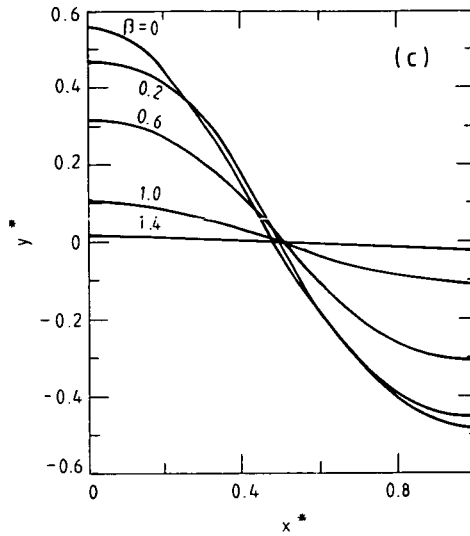


FIGURE 6 (continued)

Hence

$$\begin{aligned}
 y_{\text{nose}}^* &= -y_{\text{tail}}^* \sim \varepsilon - \frac{3}{4}\pi^3\varepsilon^3\tau \quad \text{when } 24\pi\tau \ll 1 \\
 &\sim \left(\varepsilon - \frac{3}{64}\pi^2\varepsilon^3\right) + \frac{3}{8}\pi^3\varepsilon^3\tau \quad \text{when } 24\pi\tau \gg 1.
 \end{aligned}
 \tag{15}$$

Outmans [8] has omitted the third term of equation (14) from his equation (5.2) and hence obtains the uniform increase in amplitude without predicting the initial fall. In Figure 6, predicted and calculated velocities at $\tau = 0$ agree to within 2.5 per cent for $\beta = 1$ and the corresponding displacements at $\tau = 0.6$ to within 0.05 per cent (the amplitude when $\beta = 1$ grows so slowly that we expect the perturbation solution (14) to still be valid to within $O(\varepsilon^4)$ when $\tau = 0.6$).

Since $\partial y/\partial t - V = (\alpha_1 + \alpha_2)V\partial y^*/\partial \tau$, we see from Figure 6(a) that by decreasing the wavelength of the disturbance (*i.e.* decreasing L) and hence increasing τ we increase the magnitudes of the nose and tail velocities relative to the mean flow when $\beta = 0$ and $\varepsilon = 0.1$. If we further insist that the initial dimensional amplitude εL remains fixed as we decrease L , then ε must increase which will further increase those velocities, as we can see from Figure 7(b). This growth rate/wavelength behaviour agrees with that predicted by first order theory and conflicts with conclusions of Outmans [8] who incorrectly assumes that the (small) higher order terms of his perturbation analysis are of sufficient importance to have a significant effect on the general trend set by the dominant first term. When $\beta > 0$, the growth rate/wavelength dependence is not clear since now β in addition to τ increases as L decreases, with the β -dependence tending to decrease the growth rate of the disturbance and the τ -dependence tending to increase it.

Figures 6(b) and 6(c) show the increase in the amplitude of the displacement at a given time τ as interfacial tension γ decreases (*i.e.* β decreases). Furthermore, the growth rate and displacement of the nose when $\tau = 0.6$ becomes larger than that of the tail as β approaches zero. This departure from antisymmetry which develops with time for small β can be seen in Figure 6(c) for $\beta = 0$ and to a lesser extent for $\beta = 0.2$ (the effect is also apparent in Outmans' Figure 3). Repeating the calculations of Figure 6 ($\epsilon = 0.1, \tau \leq 0.6$) with $\alpha_1 = 0.5$ reveals little change in the displacement/ τ plot except when $\beta = 0$ for which the nose is shorter by about 0.04 when $\tau = 0.6$, thereby returning closer to antisymmetry. Similar behaviour for larger values of initial amplitude ϵ is shown in Figure 7(a) for $\beta = 0$. Of course, changing α_1 must alter the displacement/dimensional time (t) dependence since $\tau = (\alpha_1 + \alpha_2)Vt/L$, and the displacement/ γ dependence since $\beta^2 = \pi^2\alpha_3/(\alpha_1 + \alpha_2)$.

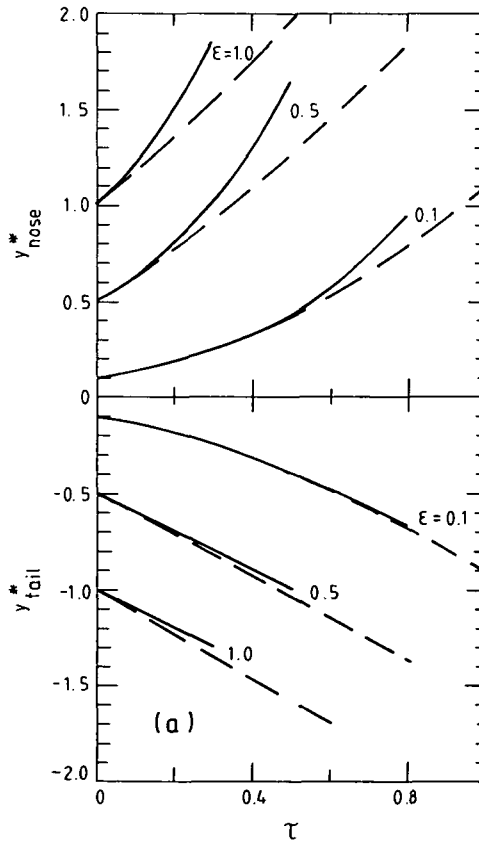


FIGURE 7. Development of an initial dimensionless displacement $y^* = \epsilon \cos \pi x^*$ with dimensionless time $\tau = (\alpha_1 + \alpha_2)Vt/L$ when $\beta = 0, \epsilon = 0.1, 0.5, 1.0, \alpha_1 = 0.5, 1.0$ where $y^* = (y - Vt)/L$ and $x^* = x/L$. (a) Dimensionless nose and tail displacements relative to the mean flow position versus τ . (b) Dimensionless nose and tail velocities relative to the mean flow versus τ . In both (a) and (b) solid lines correspond to $\alpha_1 = 1$ and dashed lines to $\alpha_1 = 0.5$.

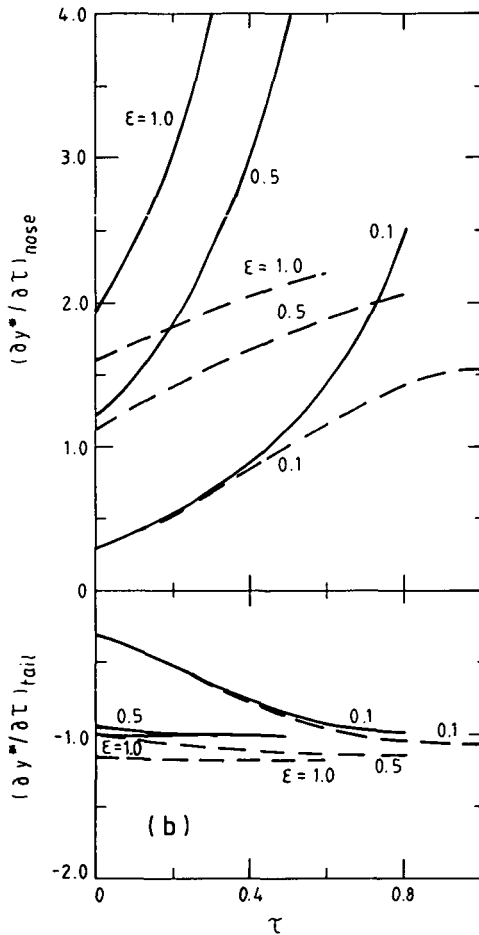


FIGURE 7 (continued)

From equation (1) we see that small sinusoidal disturbances ($\epsilon \ll 1$) initially grow like $\exp(\sigma t)$ where σ decreases with decreasing α_1 , and $\sigma t = 2\pi L\tau/\lambda$ when $\gamma = 0$; thus first order theory predicts an amplitude reduction with decreasing α_1 . In particular, it predicts that the y^*/τ curve will be independent of α_1 when $\gamma = 0$, where the fall in amplitude with α_1 occurs since $\tau = (\alpha_1 + \alpha_2)Vt/L$. The effect is somewhat different in Figure 7(a), when $\gamma = 0$ and $\epsilon = 0.5$ and 1.0; the nose becomes shorter and the tail longer for given τ , with the effect being greatest at the nose so that the amplitude at fixed τ decreases with α_1 . Similar behaviour occurs when $\epsilon = 0.1$ for τ large enough. However, the overall effect is for the amplitude at given t to decrease also with α_1 , as in first order theory.

In Figure 7(a) we see that, as the initial amplitude ϵ increases when $\beta = 0$, the departure from antisymmetry increases. This is clearer in Figure 7(b) where the nose velocity increases and the tail velocity tends to decrease with increasing ϵ ,

such changes being much greater at the nose than at the tail. Furthermore, the calculated effect at the tail diminishes with increasing τ (indeed when $\alpha_1 = 1$, tail velocities for $\varepsilon = 0.5$ and 1.0 become identical at $\tau = 0.3$). The tail velocities in Figure 7(b) appear to plateau and they become more uniform in time as ε increases; in particular, when $\varepsilon = 0.5$ and 1.0 the tail experiences an approximately linear displacement. Similarly, the nose velocity for $\alpha_1 = 0.5$ and $\varepsilon = 0.1$ also appears to plateau, although more data are needed to confirm this trend. The rapid onset of linear rates of displacement have been observed in Hele-Shaw cells by Gupta *et al.* [5] (of course, at large times when a steady finger shape is achieved, the displacement is also linear).

Calculations similar to those of Figure 7 break down for $\beta > 0$ after times $\tau = 0.2$ and 0.05 when the initial amplitude ε is 0.5 and 1.0 , respectively, and are not shown here. Since the integral equation has a computationally conservative form for $\beta = 0$ but not for $\beta > 0$, one might speculate that the discovery of such a form for $\beta > 0$ is required to achieve comparable error growth rates. As in Figure 6(b), available results for $\beta = 1$ again show an initial decrease and subsequent rise in amplitude, but the size of this minimum increases with ε for $\varepsilon = 0.1, 0.5, 1.0$.

7. Conclusion

A stepwise numerical procedure is described for tracing the evolution of a periodic interface between two immiscible fluids flowing in a two-dimensional porous medium or Hele-Shaw cell. For unstable flows the growth rate of numerical errors is reduced, through a combination of smoothing at each time step and the choice of values for the numerical parameters, and the usable part of the calculation extended to finite amplitudes which may be much greater than those for which a perturbation analysis is valid. The numerical solution for zero interfacial tension is shown to agree with the corresponding exact Saffman solution before deviating because of the associated growth of errors.

Calculations for an initial sinusoidal displacement confirm the amplitude behaviour predicted by first order theory except when $\lambda = \lambda_c$. In that case, first order theory predicts neutral stability; however our calculations show a small initial fall in amplitude followed by a slow uniform increase with time. The latter trend was first predicted by Outmans [8] who considered higher order terms in a perturbation analysis. Our calculations also confirm Outmans' conclusions that (a) the first order solution tends to overestimate the amplitude with increasing time, and (b) the disturbance departs from antisymmetry with time in the absence of interfacial tension ($\gamma = 0$). However, contrary to Outmans and in agreement

with first order theory, we find that decreasing the wavelength of the disturbance increases its growth rate when $\gamma = 0$. Finally, our calculations predict that the departure from antisymmetry when $\gamma = 0$ increases when either the initial amplitude or α_1 increases; it also decreases as γ increases.

Appendix

The following results may be derived from equations (A8) and (A9) in Davidson [3]:

$$\int_C \frac{\partial G}{\partial n(\xi)} ds(\xi) = 0, \quad (\text{A1})$$

$$\begin{aligned} \int_C \left(\cos \theta(\xi) \frac{\partial G}{\partial s(X)} + \cos \theta(X) \frac{\partial G}{\partial s(\xi)} - (\eta - \nu) \frac{\partial^2 G}{\partial s(X) \partial n(\xi)} \right) ds(\xi) \\ = \cos \theta(X) (G(X; \xi_L) - G(X; \xi_0)). \end{aligned} \quad (\text{A2})$$

In particular, equation (A2) above is obtained by splitting the integral on C in Davidson's equation (A9) into two parts, $C - C_\epsilon$ and C_ϵ where C_ϵ is a small segment, differentiating along a direction which tends to $s(X)$ as X approaches a point on C_ϵ , then taking the limit $\epsilon \rightarrow 0$ after the limit in X .

Note added in proof. Tryggvason and Aref (*J. Fluid Mech.* 136 (1983), 1–30) have recently published numerical simulations in which numerical errors were accepted as part of the solution and large-scale finger development was achieved. The author discusses the present work, with reference to Tryggvason and Aref, in a paper entitled "On the motion of the interface between two immiscible fluids in a Hele-Shaw model of a two-dimensional porous medium", presented at CSIRO/DSIR Seminar on Convective Flows in Porous Media, Wairakei, New Zealand, May 3–4, 1984 (Proceedings to appear).

References

- [1] J. H. Ahlberg, E. N. Nilson and J. L. Walsh, *The theory of splines and their applications* (Academic, New York, 1967).
- [2] R. L. Chuoke, P. van Meurs and C. van der Poel, "The instability of slow, immiscible, viscous liquid-liquid displacement in permeable media", *Trans. AIME* 216 (1959), 188–194.
- [3] M. R. Davidson "An integral equation for immiscible fluid displacement in a two-dimensional porous medium or Hele-Shaw cell", *J. Austral. Math. Soc. Ser. B* 26 (1984), 14–30.

- [4] I. S. Gradshteyn and I. M. Ryzhik, *Table of integrals, series and products, enlarged edition* (Academic, New York, 1980).
- [5] S. P. Gupta, J. E. Varnon and R. A. Greenkorn, "Viscous finger wavelength degeneration in Hele-Shaw models", *Water Resources Res.* 9 (1973), 1039–1046.
- [6] R. W. Hamming, *Numerical methods for scientists and engineers* (McGraw-Hill, New York, 1962).
- [7] M. S. Longuet-Higgins and E. D. Cokelet, "The deformation of steep surface waves on water. I. A numerical method of computation", *Proc. Roy. Soc. London Ser. A* 350 (1976), 1–26.
- [8] H. D. Outmans, "Nonlinear theory for frontal stability and viscous fingering in porous media", *Soc. Petrol. Engr. J.* 2 (1962), 165–176.
- [9] P. G. Saffman and Sir Geoffrey Taylor, "The penetration of a fluid into a porous medium or Hele-Shaw cell containing a more viscous fluid", *Proc. Roy. Soc. London Ser. A* 245 (1958), 312–329.
- [10] P. G. Saffman, "Exact solutions for the growth of fingers from a flat interface between two fluids in a porous medium or Hele-Shaw cell", *Quart. J. Mech. Appl. Math.* 12 (1959), 146–150.